colloids and interfaces

MDPI

Article

Anthocyanin-Loaded Silk Fibroin Films for Visual Detection of Volatile Bases

Nejra Omerović [1], Marija Kostić [1], Daria Ilić [1], Vladan Filipović [1] and Jaroslav Katona [2,*]

[1] BioSense Institute, University of Novi Sad, Dr Zorana Đinđića 1, 21000 Novi Sad, Serbia; nejra@biosense.rs (N.O.)
[2] Faculty of Technology Novi Sad, University of Novi Sad, Bulevar Cara Lazara 1, 21000 Novi Sad, Serbia
* Correspondence: jaroslav.katona@uns.ac.rs

Abstract

The reliability of conventional food labeling is often limited, as storage conditions during distribution cannot always be controlled, creating a need for intelligent packaging systems capable of providing real-time information on product quality. Among these, pH-responsive colorimetric indicators have attracted increasing attention, particularly those based on natural pigments such as anthocyanins, due to their biocompatibility, safety, and pronounced color changes over a wide pH range. Red cabbage extract (RCE), rich in anthocyanins, represents a promising, low-cost natural indicator, while silk fibroin (SF), a biodegradable and biocompatible protein, offers a suitable matrix for sustainable packaging materials. In this study, SF-based films incorporating water-extracted RCE were developed as pH-sensitive indicators, with polyethylene glycol 200 added as a plasticizer to enhance film performance. The films were characterized in terms of morphology, chemical and thermal properties, and colorimetric response to ammonia vapors and changes in the headspace atmosphere during chicken meat storage. The plasticized film exhibited improved structural uniformity and a more pronounced and rapid color response. Furthermore, during chicken meat storage, the film demonstrated a clear visual response that correlated with ammonia concentration in the headspace. These findings indicate that plasticized films have potential as environmentally friendly, on-package colorimetric indicators responsive to ammonia.

Keywords: silk fibroin; protein films; pH-sensitive films; intelligent packaging

1. Introduction

Food products may be stored under variable and not always strictly controlled environmental conditions during distribution from production to the end consumer. Consequently, the best-before date indicated on the packaging does not necessarily provide reliable information regarding the actual quality and safety of the packaged product. For both health and economic reasons, it is essential that consumers are able to assess whether a product is safe for consumption [1]. This need has driven the development of intelligent packaging systems. Intelligent packaging monitors the condition of packaged food and provides real-time information on product quality during transportation and storage [2]. Intelligent packaging systems can indicate changes in environmental parameters (e.g., temperature and pH), detect physical package damage, or signal microbial growth. A representative example of intelligent packaging is an on-package colorimetric indicator, primarily intended for simple consumer use [3,4].

Meat is widely consumed as a highly nutritious food rich in proteins, lipids and essential micronutrients. However, these nutrients also make it susceptible to microbial spoilage

Check for updates

Academic Editor: Akmal Nazir

Received: 18 September 2026
Revised: 9 November 2026
Accepted: 16 November 2026
Published: 18 November 2026

Copyright: © 2026 by the authors. Licensee MDPI, Basel, Switzerland. This article is an open access article distributed under the terms and conditions of the Creative Commons Attribution (CC BY) license.

during storage and distribution. Microbial metabolism leads to the degradation of proteins and lipids, resulting in the formation of various volatile and non-volatile compounds, including ammonia, biogenic amines, organic acids, aldehydes, and sulfur-containing compounds [5,6]. These biochemical transformations are accompanied by an increase in pH, the development of off-odors and off-flavors, discoloration, and textural changes, ultimately rendering the meat unacceptable for consumption [7]. Among spoilage metabolites, ammonia and other volatile basic nitrogen compounds are particularly important indicators of meat deterioration because they directly reflect the extent of protein decomposition and microbial activity. Therefore, monitoring the accumulation of these compounds and pH changes may provide useful information for assessing changes associated with meat spoilage. For this purpose, pH-sensitive indicators can be effectively applied [7–9].

pH-sensitive colorimetric indicators, consisting of dyes incorporated into polymer matrices, have attracted increasing interest as efficient and user-friendly systems for monitoring environmental changes through visible color responses. Particular emphasis has been placed on natural colorants due to their biocompatibility, low toxicity, and environmental sustainability. Among these, anthocyanins have been extensively investigated. Anthocyanins are water-soluble phenolic compounds abundantly present in fruits, vegetables, and flowers [10]. Anthocyanins exhibit pronounced and reversible color variations across a broad pH range, arising from structural transformations between flavylium cation, quinoidal base, carbinol pseudobase, and chalcone forms [10–12]. In addition to their distinct colorimetric response, anthocyanins possess antioxidant and antimicrobial properties, further enhancing their functionality. Ahmed at al. [13] developed cellulose-based indicators containing anthocyanins extracted from plum peels and demonstrated that their color changes during chicken meat storage were accompanied by increase in total volatile basic nitrogen (TVB-N), meat pH, and microbial load. Similarly, a recent study using composite anthocyanin-based films showed visible color changes during refrigerated chicken meat storage, with volatile compounds released during spoilage identified as important contributors to the indicator response [14]. Potential of anthocyanin-based biopolymer materials for the visual monitoring of meat freshness and the need for further improvements in their sensitivity and stability were reviewed by Xiong et al. [15].

Red cabbage extract (RCE) has been widely explored as a rich and accessible source of anthocyanins and as a natural colorant in food industry. RCE contains a complex mixture of anthocyanin derivatives, predominantly cyanidin-based compounds. Its broad pH-dependent color changes—from red under acidic conditions to purple and blue and eventually to green and yellow in alkaline environments—make RCE a suitable natural colorimetric indicator for intelligent food packaging [16].

In the food packaging industry, there is also a growing tendency to replace petroleum-based materials with biocompatible and biodegradable polymers derived from renewable sources, such as proteins, polysaccharides and lipids [2]. Silk fibroin (SF) is a protein that shows significant potential for advanced food packaging application, since it has been approved as a biomaterial by the U.S. Food and Drug Administration (US FDA) [17]. The most extensively studied SF is produced by silkworms of the *Bombyx mori* species. *Bombyx mori* silkworm cocoon fibers consist of approximately 70–80% fibroin and 20–30% sericin, with trace amounts of waxes, carbohydrates, pigments, and inorganic substances [18–20]. Sericin acts as an adhesive, binding strongly to the outer surface of fibroin, thereby protecting it and maintaining cocoon structural integrity [19,20]. Before SF is processed into different forms, such as nanoparticles, films, gels, and powders, sericin is typically removed in a process called degumming [21]. One of the most commonly used degumming approaches involves boiling cocoons under acidic or alkaline conditions [20,22].

Due to its favorable properties, SF has been extensively investigated for biomedical applications, including tissue engineering and controlled drug delivery [17,21,23,24]. SF has also been explored as a supporting substrate for electrochemical sensors that can be attached to a wide range of surfaces, such as human skin, plants, paper, and textiles [25]. Because SF is odorless and tasteless, it is also suitable for processing into edible coatings that can be applied directly to food surfaces. Such coatings are mostly used for highly perishable fruits (e.g., strawberries, raspberries, and bananas), extending freshness by slowing down respiration and preventing dehydration [26].

Although anthocyanins from RCE have been extensively investigated as pH-sensitive indicators in various biopolymer matrices, studies specifically combining SF with RCE remain limited, particularly in the context of intelligent food packaging applications. Several reports support the compatibility of anthocyanins with SF-based matrices and indicate that SF can protect and stabilize anthocyanins [27–29]. Ma and Jing [27] reported that self-assembled SF nanofibrils improved the thermal stability of black-rice anthocyanins. Li et al. [28] showed that SF peptides improved the physicochemical stability of cyanidin-3-O-glucoside; and Giang et al. [29] developed SF nanoparticles for heat-stable delivery of *Clitoria ternatea* anthocyanins. Xia et al. [30] reported an active colorimetric bilayer membrane for food packaging consisting of a hydrophilic SF–bayberry anthocyanin layer and a hydrophobic PCL/eucalyptus-oil layer; the membrane exhibited pH-sensitive and reversible color response, enabling freshness monitoring while also extending shelf life. Matzeu et al. [31] embedded anthocyanins extracted from blueberries and red cabbage into SF formulations to produce coated oral devices and cast edible color-changing candies. Liu et al. [32] developed pH-visualizing SF–sericin hydrogels loaded with natural anthocyanins and integrated them as thin hydrogel films in diapers for real-time urine pH indication, showing distinct color changes across different pH values.

This study presents the development of pH-sensitive colorimetric indicator films from SF isolated from *Bombyx mori* cocoons and water-extracted RCE and investigates their response to volatile ammonia and changes in the headspace atmosphere during chicken meat storage. A water-based RCE extraction approach was used, avoiding conventional solvent-based extraction. Particular attention was given to the influence of film formulation on sensing behavior and structural integrity, including the role of PEG 200 as a plasticizer (recognized as suitable for food-contact materials by the US FDA). Furthermore, the behavior of the developed films during chicken meat storage was evaluated by monitoring color changes alongside preliminary measurements of ammonia-associated membrane inlet mass spectrometry (MIMS) signal. Although SF–anthocyanin-based indicators have been previously reported, the specific contribution of this study lies in the comparative evaluation of the effect of PEG 200 on the structural and sensing properties of SF-RCE films, together with the assessment of their response under controlled ammonia exposure and during chicken meat storage. This combined approach provides additional insight into the formulation-dependent performance of SF-based colorimetric indicators and their potential application in intelligent food packaging.

2. Materials and Methods

2.1. Materials

Cocoons of *Bombyx mori* silkworm from China were used as a source of fibroin. Sodium carbonate (Na_2CO_3), sodium bromide (NaBr) and potassium chloride (KCl) were purchased from Carl Roth (Karlsruhe, Germany). Lithium bromide (LiBr; anhydrous, 99%) and sodium acetate (CH_3COONa) were procured from Thermo Fisher Scientific (Geel, Belgium). Dialysis membrane with molecular weight cut-off of 14,000 Da, polyethylene glycol 200 (PEG 200), ammonium hydroxide (NH_4OH), sodium hydroxide (NaOH) and

hydrochloric acid (HCl, 37%) were obtained from Sigma Aldrich (St. Luis, MO, USA). Anthocyanins were extracted from red cabbage supplied from a local supermarket (Novi Sad, Serbia). Fresh chicken breast was also purchased from a local supermarket (Novi Sad, Serbia). Deionized water was used in all experiments.

2.2. SF Solution Preparation

SF was extracted from *Bombyx mori* silkworm cocoons, and SF solution was prepared following the protocol published in [21]. The first step in preparing an SF solution from silkworm cocoons is the removal of sericin. Sericin was removed by boiling cut pieces of silkworm cocoons for 30 min in a 0.5% (*w*/*v*) sodium carbonate aqueous solution. During boiling, sericin dissolves, while SF remains insoluble in the form of fibers. The fibers were then rinsed for 30 min in deionized water heated to 40 °C under constant magnetic stirring. To ensure complete sericin removal, the boiling and rinsing steps were repeated three times. After the final rinse, the SF fibers were thoroughly squeezed, spread on aluminum foil, and left to dry overnight in a fume hood.

The dried SF fibers were dissolved in a 9.3 M aqueous lithium bromide solution at 60 °C for 90 min, yielding a 10% (*w*/*v*) SF solution. The resulting solution was dialyzed against deionized water using the dialysis membrane to remove Li^+ and Br^- ions. Dialysis was performed at room temperature for approximately 30 h under constant stirring. The dialyzed SF solution was then centrifuged at 10,000 rpm for 20 min to remove impurities. The SF concentration in the solution was determined by the Bradford method [33] using bovine serum albumin as a standard. The SF solution was stored at 4 °C until further use for film preparation.

2.3. RCE Preparation

The method for preparing RCE was adopted from [1] and slightly modified based on preliminary experiments evaluating the amount and stability of the extracted anthocyanins. Red cabbage was chopped using a manual chopper and mixed with water in a red cabbage-to-water ratio of 1:2 (*w*/*v*). Extraction was performed at 100 ± 2 °C for 20 min, followed by cooling to approximately 40 °C. To remove plant material, the extract was first filtered through four layers of cotton gauze (20 threads/cm^2). The extract was then centrifuged at 10,000 rpm for 10 min and filtered through quantitative filter paper (Whatman grade 41) to remove fine suspended impurities. The filtrate was collected in plastic Falcon tubes, wrapped in aluminum foil, and stored in the refrigerator until use. No additional purification steps were applied to the RCE; therefore, the extract is expected to contain various co-extracted components in addition to anthocyanins, such as sugars, sugar alcohols, and amino acids [16].

2.4. Determination of Total Monomeric Anthocyanin Concentration (TMAC) in RCE

The total monomeric anthocyanin concentration (TMAC) in RCE was determined using the pH-differential method [10]. This method is based on pH-dependent structural transformations of the anthocyanin chromophore and, therefore, on absorbance measurements at pH 1.0 and 4.5. RCE was appropriately diluted with 0.025 M potassium chloride buffer (pH 1.0) and 0.4 M sodium acetate buffer (pH 4.5), and absorbance was measured at 520 nm (λ_{max}) and 700 nm using a double-beam UV–Vis spectrophotometer, Jasco V-750 (Jasco, Tokyo, Japan). All measurements were performed 15–60 min after preparation of dilutions. Deionized water was used as the blank. The TMAC was calculated using Equation (1) and expressed as cyanidin-3-glucoside (cyd-3-glu) equivalents:

$$\mathrm{TMAC}\left(\frac{\mathrm{mg}}{\mathrm{l}}\right) = \frac{\mathrm{A} \times \mathrm{Mw} \times \mathrm{DF} \times 1000}{\varepsilon \times \mathrm{l}} \quad (1)$$

where A is absorbance, calculated as $A = [(A_{520} - A_{700})_{pH=1.0} - (A_{520} - A_{700})_{pH=4.5}]$; Mw is the molecular weight of cyd-3-glu (449.2 g/mol); *DF* is the dilution factor, calculated as DF = final volume/initial volume (DF = 30); ε is the molar extinction coefficient for cyd-3-glu (26,900 L cm^{-1} mol^{-1}); l is the cell pathlength (1.0 cm); and 1000 is the conversion factor from g to mg.

2.5. pH-Dependent UV–Vis Spectra and Color Changes of RCE

The spectral characteristics and color changes of RCE were evaluated over the pH range of 1–13. RCE dilutions (DF = 20) were prepared, and pH was adjusted using 1.0 M and 0.1 M HCl and 1.0 M and 0.1 M NaOH solutions. Absorption spectra were recorded in the 400–800 nm wavelength range using a UV–Vis spectrophotometer, Jasco V-750 (Jasco, Tokyo, Japan). Photographs of the corresponding RCE dilutions were also taken.

2.6. Film Preparation

Films were prepared by the solvent casting technique. To prepare the film-forming solution, the pH of the 6 g 3% SF aqueous solution was adjusted to 3, and 6 g of RCE was added, followed by stirring for 15 min. PEG 200, 20% (*w*/*w*) based on SF weight, was then added, and the mixture was stirred for an additional 15 min. After homogenization and pH readjustment, if necessary, 12 g of film-forming solution was cast into round PTFE Petri dishes (6 cm in diameter) and dried at 40 °C for 16 h to allow for solvent evaporation and film formation (films labeled SF-RCE-PEG). After drying, the films were conditioned at room temperature in a desiccator at 60 ± 2% relative humidity (RH; maintained using a saturated sodium bromide solution) for 2 h. The films were then peeled from the Petri dishes and stored at ambient temperature and humidity, protected from light. Prior to each analysis, the films were reconditioned at 60 ± 2% RH for 2 h. Films were also prepared without PEG 200 and/or RCE and were denoted SF-RCE and SF films, respectively.

2.7. Scanning Electron Microscopy (SEM)

The microstructure of *Bombyx mori* silk fibers before and after degumming, as well as the surface and cross-sectional morphologies of the films, were examined using a Thermo Scientific Apreo^{TM} 2C scanning electron microscope (Thermo Fisher Scientific, Waltham, MA, USA). Samples were mounted to aluminum stages using double-sided carbon adhesive tape. Images were acquired at a low accelerating voltage (1–2 kV).

2.8. Film Thickness

The thickness of the films was measured using a digital micrometer (Mitutoyo Corp., Tokyo, Japan) and reported as the mean of 10 measurements taken at different positions on each film.

2.9. Thermogravimetric Analysis (TGA)

Thermogravimetric analysis (TGA) was used to investigate the thermal properties of the developed films. TGA was performed using a Netzsch 449 F5 Jupiter simultaneous thermal analyzer (Netzsch, Selb, Germany). Approximately 12 mg of film sample was placed in an aluminum oxide crucible and heated from 30 °C to 800 °C, at a heating rate of 10 °C/min and under a constant nitrogen flow of 30 mL/min. Netzsch Proteus 8.0 software was used to analyze the thermograms and calculate the first derivative.

2.10. Fourier-Transform Infrared-Attenuated Total Reflectance (FTIR-ATR) Spectroscopy

The chemical composition of the films and possible intermolecular interactions among their components were analyzed by FTIR-ATR spectroscopy. The spectra were recorded

using a Jasco FT/IR 6600 FTIR spectrometer (Jasco, Tokyo, Japan) in the spectral range of 4000–500 cm^{-1} at a resolution of 4 cm^{-1}.

2.11. Color Analysis

Film color was quantified in the CIE Lab color space using reflectance data, as described in [34]. Reflectance spectra of film samples were measured using a Jasco V-750 UV–Vis spectrophotometer (Jasco, Tokyo, Japan) over the 350–800 nm wavelength range, with a 1 nm step. In the CIE Lab system, color is defined by three coordinates: L*—lightness (0 is black, and 100 is white); a*—green-red axis (negative values indicate green, and positive values indicate red); and b*—blue-yellow axis (negative values indicate blue, and positive values indicate yellow).

The L*, a*, and b* values were calculated from the recorded reflectance following the methodology described in CIE Standard Observers and calculation of CIE X, Y, Z color values [35]. To obtain color values representative of daylight conditions (correlated color temperature of about 6504 K), the CIE D65 standard illuminant [36] was chosen and multiplied with the reflectance spectrum. The X, Y, and Z tristimulus values, corresponding to the CIExyz color space, were then calculated by multiplying the resulting spectrum by their respective CIE 1931 color-matching functions (2-degree observer) [37] and integrating the obtained curves over the 360–800 nm wavelength range, as given in Equation (2):

$$V_i = \sum_{w=360\ nm}^{800\ nm} R_{sample} \cdot I_{CIE65} \cdot C_i, i \in \{X, Y, Z\} \quad (2)$$

where V_i is the value of X, Y or Z; R_{sample} is the measured reflectance spectrum; I_{CIE65} is the CIE D65 standard illuminant curve; and C_i is the respective color-matching function.

Finally, CIExyz values were converted into the CIE Lab color space using the scikit-image Python 0.22.0 package [38], again applying D65 illuminant and 2-degree observer conversion settings. The accuracy of the computed colors was additionally verified by visual inspection by converting the values into the RGB color space and displaying them on a color-calibrated display. This way it was confirmed that the calculated values accurately represented the color of the film samples.

Euclidean distance in the CIE Lab color space, i.e., the total color difference (ΔE), was calculated using Equation (3):

$$\Delta E = \sqrt{(L^* - L_0)^2 + (a^* - a_0)^2 + (b^* - b_0)^2} \quad (3)$$

where L^*, a^*, and b^* are the color parameters of the tested film samples and L_0, a_0, and b_0 are the color parameters of the reference film sample, i.e., before the test.

2.12. Colorimetric Response of Indicator Films to Ammonia Vapors

The sensitivity of indicator films to ammonia vapor was evaluated using the approach in [39], with slight modifications. Briefly, 20 mL of 0.1 M ammonia solution was placed in a Petri dish (9 cm in diameter), and an indicator film strip (3.5 cm × 1.0 cm) was attached to the inner side of the lid and exposed to the headspace. Film reflectance spectra were recorded with a Jasco V-750 UV–Vis spectrophotometer (Jasco, Tokyo, Japan) over the 350–800 nm wavelength range before exposure and after 3, 5, 10, 15, 20, 25, 30, 40, 50, 60, 90, and 120 min of exposure to ammonia vapor. Color parameters were calculated from the reflectance data as described in the previous section. To prevent mechanical damage during handling and measurements, the film strips were mounted on a transparent plastic sheet, which also served as the reference for reflectance recordings.

2.13. Potential Application of Indicator Films for Monitoring Chicken Meat Freshness

2.13.1. Determination of Ammonia Concentration

To monitor ammonia production associated with meat spoilage, chicken breast meat was used as a real food matrix, and ammonia was quantified by MIMS according to the method reported in [34].

The experimental setup consisted of a portable mass spectrometry system equipped with a membrane-based sample inlet, a Prisma Plus® compact mass spectrometer (Pfeiffer Vacuum GmbH, Aßlar, Germany), a vacuum system with diaphragm and turbomolecular pumps, and a laptop computer for instrument control, data acquisition, and data processing. The system was integrated with a sheet membrane probe. The stainless-steel probe was custom-built and combined with an SIL-TEC A class VI USP medical-grade polydimethylsiloxane (PDMS) sheet membrane to enable selective introduction of volatile organic compounds (VOCs) into the system. The membrane thickness was 0.125 mm, and the active membrane area was 32 mm^2.

Prior to meat analysis, an NH_3 calibration curve was established using the MIMS device. In MIMS, volatile compounds from the sample permeate continuously through a semi-permeable membrane directly into the vacuum system of the mass spectrometer, where they are ionized and detected by their mass-to-charge (m/z) ratio, enabling rapid, real-time quantification of gaseous species. Ammonia calibration solutions of different concentrations (1%, 5%, 10%, and 25% (v/v)) were prepared in 1000 mL glass bottles. Clean air served as the reference, and the characteristic ions in the mass spectrum for NH_3 were monitored. To ensure consistent evaporation, the bottles were pre-equilibrated in a drying oven at 35 °C prior to measurement. The maximum ion current intensities for dominant NH_3 peaks (masses 17, 16, and 15) were recorded and converted into ppm using the known percentage of ammonia in the evaporated standards.

Ammonia formation during meat spoilage was monitored by placing 100 g of fresh chicken breast meat in a 1000 mL glass bottle equipped with a custom-designed valve cap to prevent air leakage during analysis. The bottle was maintained at 25 °C in a temperature-controlled chamber, and headspace measurements were performed by the MIMS device over a 96 h period at predetermined time points. For each measurement, the bottle's valve outlet was connected to the membrane probe using PTFE tubing. In total, 11 measurements of NH_3 were acquired during the 96 h monitoring period, using a single experimental sample, without independent replicates. The NH_3 signal was evaluated by tracking its dominant ions in the mass spectrum, and each recording lasted approximately 15 min, during which the concentration of detected ammonia reached its maximum value.

2.13.2. Colorimetric Response of Indicator Films

To evaluate the applicability of the indicator films for monitoring meat freshness, 15 g of chicken breast was placed in a Petri dish (9 cm in diameter), maintaining the same container volume-to-meat mass ratio as in the MIMS experiment. Indicator films were cut into strips (3.5 cm × 1.0 cm) and attached to the inner side of the Petri dish lid. Film color changes were monitored over 96 h by recording reflectance spectra daily using a Jasco V-750 UV–Vis spectrophotometer (Jasco, Tokyo, Japan) over the 350–800 nm wavelength range. Color parameters were calculated from the reflectance data as described previously, and ΔE was calculated using Equation (3). To prevent mechanical damage during handling and measurements, the film strips were mounted on a transparent plastic sheet, which also served as the reference for reflectance recordings. All tests were performed at room temperature (25 °C), using three independent samples.

2.14. Statistical Analysis

The analyses were performed by taking three replicates, and results are expressed as averages ± standard deviations. Experimental data were analyzed by single-factor analysis of variance (ANOVA) with a significance level of 0.05. Significantly different results ($p < 0.05$) were compared through Tukey's Honest Significant Difference (HSD) test.

3. Results and Discussion

3.1. Microstructure of Silk Fibers

SEM micrographs illustrating the microstructure of *Bombyx mori* silk fibers before and after sericin removal using sodium carbonate are shown in Figure 1. In the micrographs of fibers before degumming, as shown in Figure 1(a_1,a_2), the characteristic paired fibroin brins bound together by sericin are visible [40–42]. The fiber surfaces appeared mostly smooth and continuous; however, local irregularities were present where the sericin layer was partially detached, exposing clearly distinguishable fibroin filaments, as shown in Figure 1(a_2).

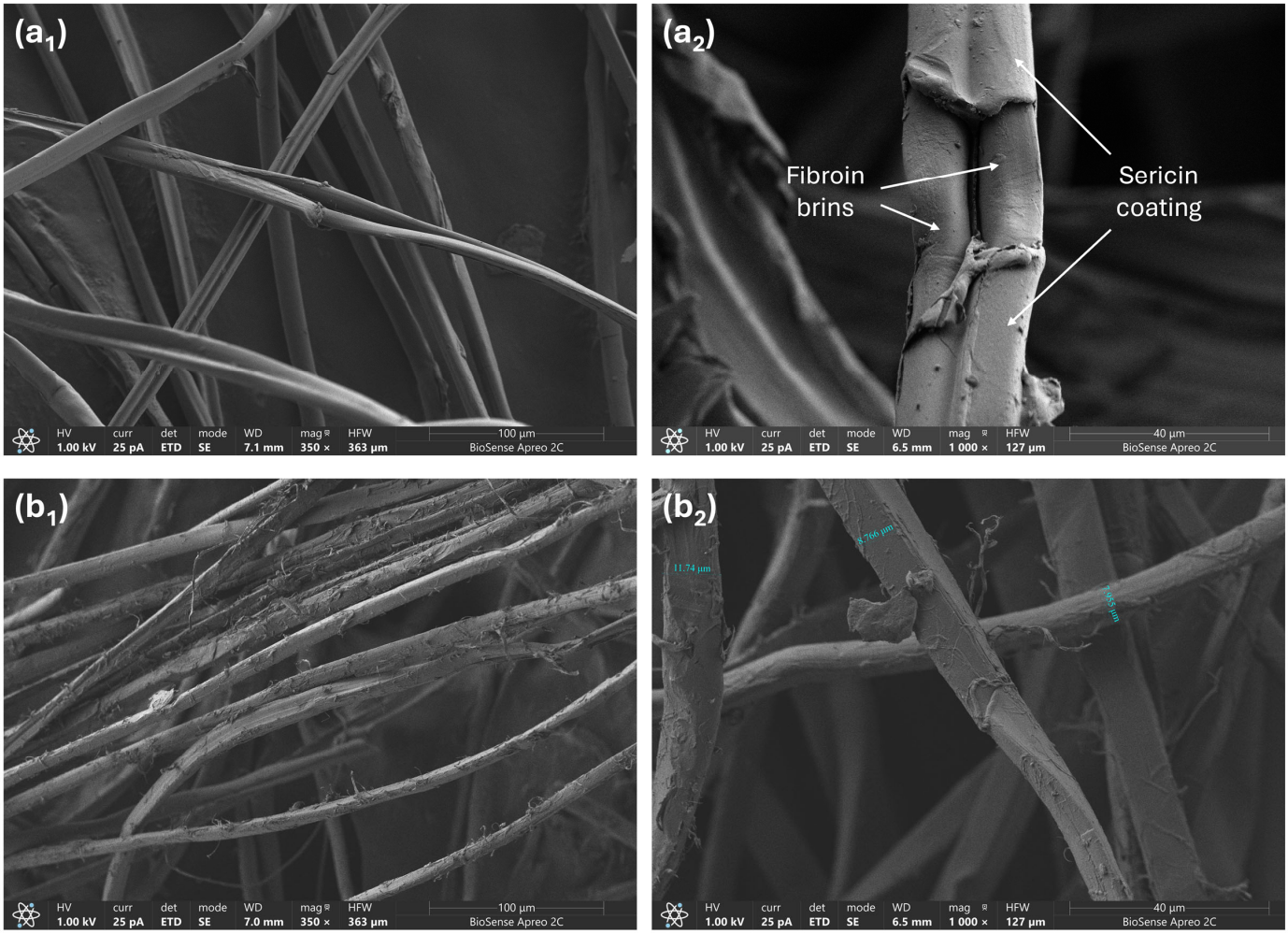


Figure 1. SEM images of *Bombyx mori* silk fibers (**a**) before and (**b**) after degumming; (**1**) 350× magnification and (**2**) 1000× magnification.

In the micrographs of degummed silk fibers, as shown in Figure 1(b_1,b_2), separation of the paired fibroin brins into individual filaments can be observed [42,43]. As shown in the higher-magnification image, Figure 1(b_2), the measured fiber diameters were approximately

8–12 µm, which is within the range reported for degummed silk fibroin filaments [43]. Compared with the raw fibers, the degummed fibers exhibited a rougher surface with localized damage, including longitudinal peeling and detached fragments. These observations indicate effective sericin removal, although alkaline hydrolysis induced by sodium carbonate likely caused slight surface degradation of fibroin [43].

3.2. TMAC, Color and Spectral Properties of RCE

The TMAC in RCE was 505.24 ± 0.03 mg cyd-3-glu/l. The coloration of RCE dilutions from pH 1 to pH 13 is shown in Figure 2a. The color changes observed in Figure 2a correspond to structural transformations in anthocyanin molecules in response to acidity or alkalinity of the environment. Under strongly acidic conditions (pH 1–2), anthocyanins predominantly exist in flavylium cation form [10,12,16], which gives a red color to RCE. As pH slightly increases, deprotonation of the flavylium cation occurs, producing a pink hue at pH 3. At pH 4–6, hydration reactions lead to less intensely colored RCE solutions (pale pink to pale purple). At pH 7, anthocyanins mainly exist in neutral quinoidal base form, giving a purple color. With further increase in pH (pH 8), additional deprotonation transforms anthocyanins into anionic quinoidal bases, which appear blue [10,12,16]. At pH 9–10, the color of RCE solution transitions toward green. At high pH values (≥11), anthocyanins undergo structural rearrangements and further deprotonation, eventually forming chalcone structures and resulting in yellow coloration [10,12,16].

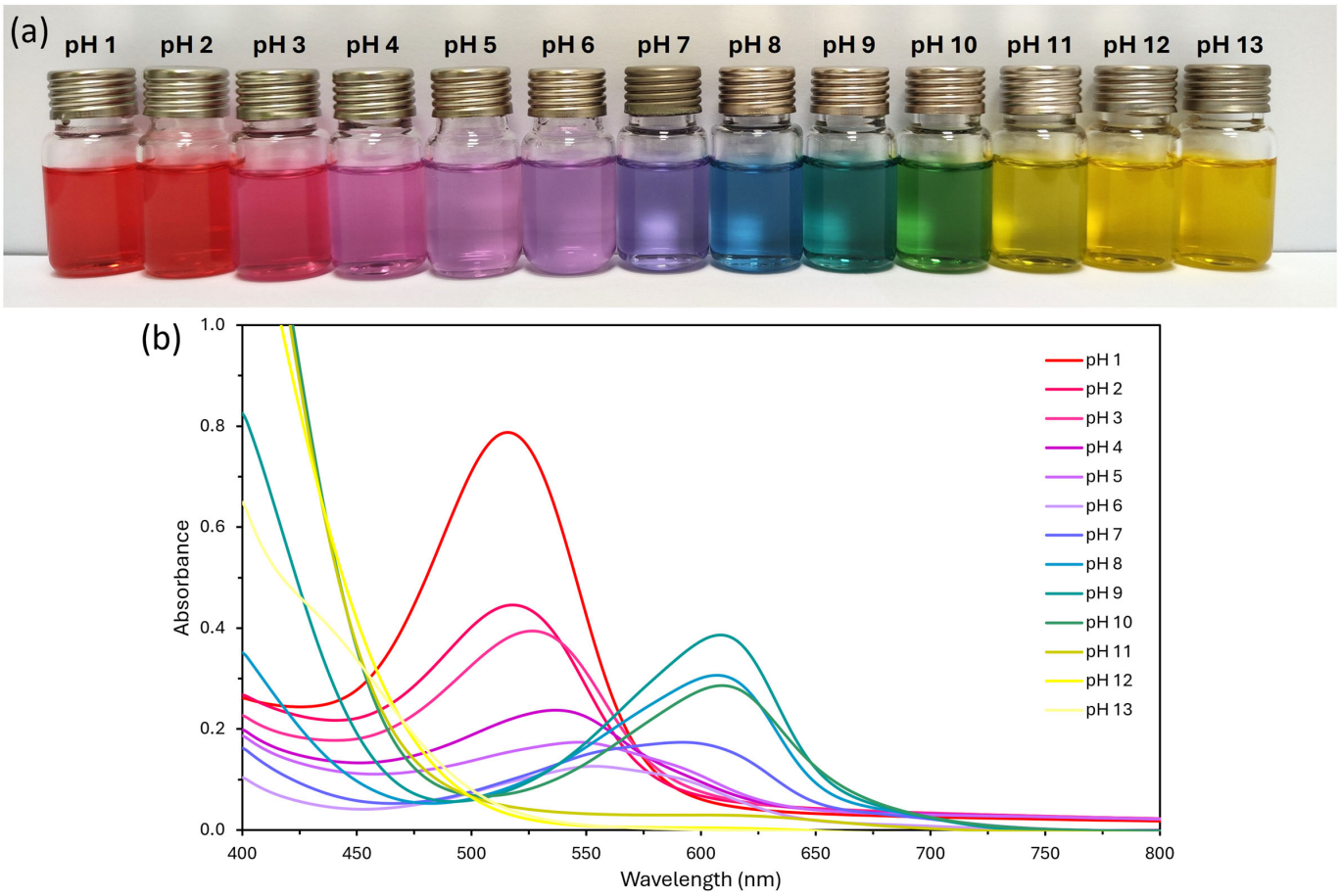


Figure 2. Color variation (**a**) and absorption spectra in the visible range (**b**) of the RCE solutions from pH 1 to pH 13.

The described structural transitions in anthocyanin molecules and the corresponding color changes were supported by the absorption spectra of the RCE solutions recorded over the same pH range, as shown in Figure 2b. In highly acidic environments (pH 1–2), a strong absorption peak with a maximum at approximately 520 nm was observed. With increasing pH, the peak intensity steadily decreased, and the maximum shifted to higher wavelengths, reaching 553 nm at pH 6. At pH 7, a notable bathochromic shift occurred, with the absorption maximum moving to 592 nm. With further increase in pH the absorption peak shifted to higher wavelengths, reaching the maximum wavelength of 608 nm at pH 10. The absorbance increased gradually from pH 7 to 9. Subsequently, at pH 10 the absorbance began to decrease again. The absorbance peak became progressively flattened and nearly disappeared by pH 12. These results are consistent with literature reports and confirm the suitability of water-based RCE as a pH-responsive colorant [10–12,16].

3.3. Film Characterization

3.3.1. Morphology

The cross-sectional morphology and air-facing surfaces of the SF films were examined by SEM, and micrographs are shown in Figure 3. The cross-sectional micrographs of the pure SF film, as shown in Figure 3(a_1,a_2), revealed a dense, compact, pore-free internal structure, indicating the efficient arrangement and close packing of SF chains and successful film formation during solvent evaporation [44–46]. The fracture surface was cohesive and slightly rough, with layered features typical of brittle rupture of a compact protein matrix, likely originating from sample preparation for SEM analysis. The neat SF film also exhibited a continuous and relatively smooth surface with only slight undulations, as can be seen in Figure 3(a_3).

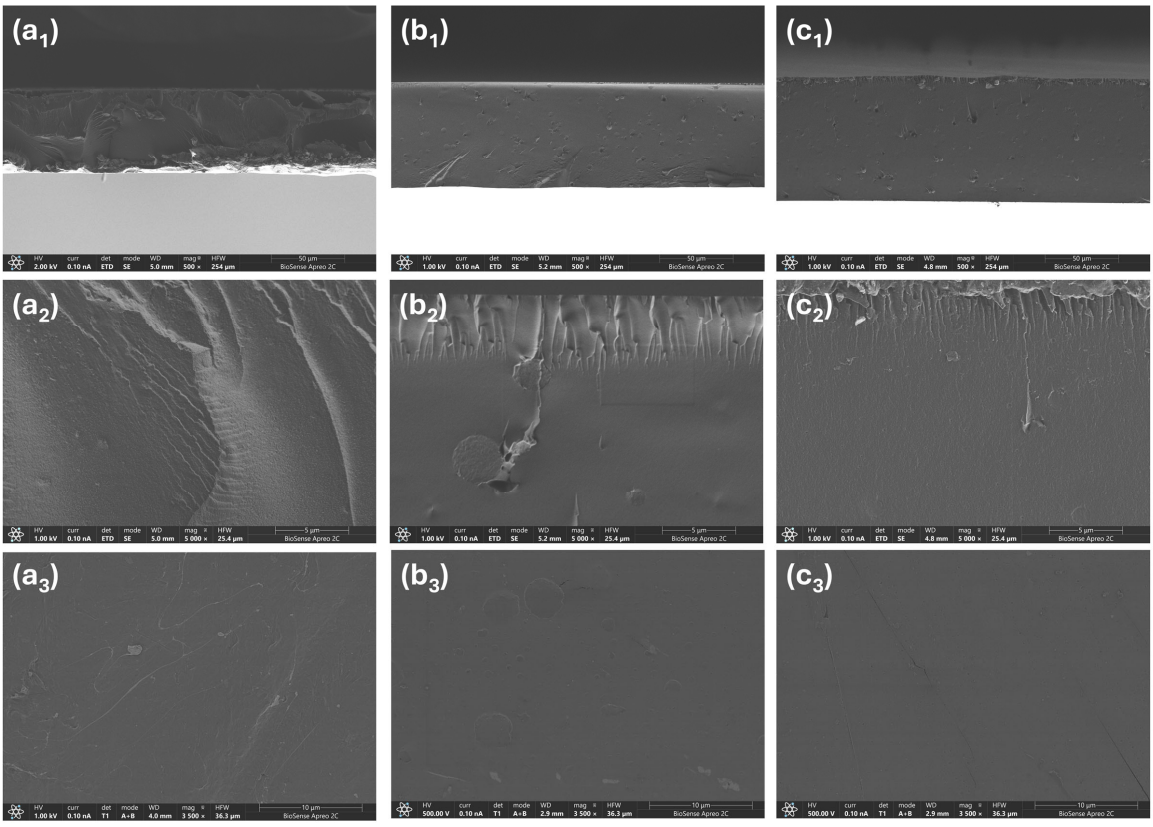


Figure 3. SEM images of (**a**) SF, (**b**) SF-RCE, and (**c**) SF-RCE-PEG films; (**1**) cross-section at 500× magnification, (**2**) cross-section at 5000× magnification, and (**3**) surface at 3500× magnification.

After incorporation of RCE, as shown in Figure 3(b_1,b_2), the cross-section remained largely compact; however, globular dispersed heterogeneities were visible within the film matrix, and stratification with elongated, vertically oriented features was observed in the upper region of the film. This localized heterogeneity may be attributed to partial incompatibility of RCE components with the SF network. The fracture surface appeared relatively smoother than that of the pure SF film, indicating changes in film morphology following RCE incorporation. On the SF-RCE film surface, circular irregularities of different sizes were also observed, as shown in Figure 3(b_3).

Upon further addition of PEG 200, as shown in Figure 3(c_1,c_2), the rounded aggregate formations and stratification were reduced, suggesting a more uniform distribution of RCE within the SF matrix [8,47]. The SF-RCE-PEG film also exhibited a more uniform surface, with no major defects, as shown in Figure 3(c_3).

3.3.2. Thickness

The thickness values of the obtained films are presented in Table 1. Film thickness increased progressively with the incorporation of RCE and PEG 200. The pure SF film had an average thickness of 54 µm, whereas the addition of RCE increased the thickness to 72 µm, and the subsequent incorporation of PEG 200 resulted in the thickest film of 87 µm. This trend can also be observed in the cross-sectional SEM micrographs acquired at lower magnification, as shown in Figure 3(a_1,b_1,c_1). The increase in thickness can be attributed to the higher amount of non-volatile compounds in the film-forming solutions [9,48,49]. Since the films were cast over the same surface area, the higher total solid content remaining after drying could contribute to the formation of thicker films.

Table 1. Film thickness. Different letters indicate a statistically significant difference ($p < 0.05$).

Film	SF	SF-RCE	SF-RCE-PEG
Thickness (µm)	54.43 ± 2.21 [a]	72.20 ± 2.82 [b]	87.37 ± 3.71 [c]

3.3.3. Thermal Stability

The thermogravimetric (TG) and derivative thermogravimetric (DTG) curves of the obtained films are shown in Figure 4 and were used to evaluate the effects of RCE and PEG 200 on film thermal stability. All samples exhibited a multistep thermal degradation profile.

For the neat SF film, as shown in Figure 4a, no pronounced degradation occurred below 200 °C. The SF film showed only a slight initial mass loss between approximately 80 and 150 °C, which can be attributed to the evaporation of physically adsorbed and bound water [42,50,51]. The main mass loss of the SF film occurred in the 270–400 °C range, with the maximum degradation rate (DTG peak) at 284 °C, primarily associated with breakage of peptide bonds in the fibroin polypeptide chains [42,51,52]. Between 400 °C and 550 °C, mass loss proceeded more gradually, followed by a further decline at higher temperatures, leaving a small residue of approximately 3% at 800 °C.

The SF-RCE and SF-RCE-PEG films, as shown in Figure 4b,c, began to degrade at lower temperatures, particularly in the 120–200 °C region, and both displayed a pronounced DTG peak at 156 °C, indicating the presence of thermally less stable components introduced by the RCE [53]. This behavior may also be related to the weakened intermolecular interactions and increased chain mobility upon addition of RCE and PEG 200 [54]. The DTG curves of the SF-RCE and SF-RCE-PEG films showed a second degradation stage centered at 306 °C and 294 °C, respectively, corresponding to decomposition of the fibroin-based matrix. The shift in this stage toward higher decomposition temperatures may be associated with hydrogen bonding between RCE components and the fibroin matrix [3]. The SF-RCE film exhibited a

broader and more complex degradation profile than the SF and SF-RCE-PEG films, with additional degradation regions at higher temperatures and a residue of 6% at 800 °C. In contrast, the SF-RCE-PEG film retained a substantially higher residue of 31% at 800 °C. Although these differences may reflect variations in the degradation pathways and thermal persistence of carbonaceous residues, their underlaying mechanisms cannot be established from the present TG-DTG data alone.

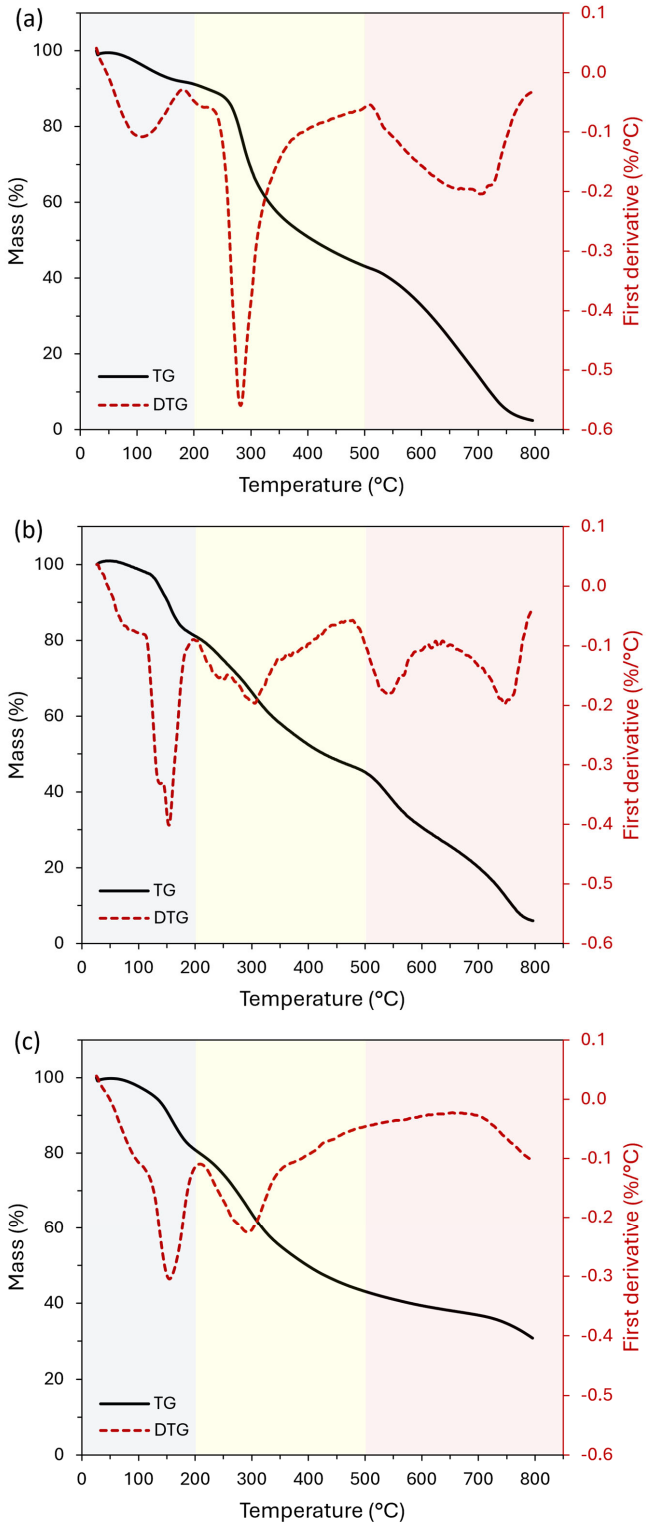


Figure 4. TG and DTG curves of (**a**) SF, (**b**) SF-RCE, and (**c**) SF-RCE-PEG films.

3.3.4. FTIR-ATR Analysis

Intermolecular interactions within the films were investigated by FTIR-ATR spectroscopy. The FTIR-ATR spectra of SF, SF-RCE, and SF-RCE-PEG films are shown in Figure 5. All films exhibited the characteristic protein bands in the 3200–3400 cm^{-1}, 2850–3000 cm^{-1}, 1620–1660 cm^{-1}, 1510–1540 cm^{-1}, and 1220–1260 cm^{-1} regions, which were attributed to O–H and N–H stretching, C–H stretching, amide I, amide II and amide III, respectively [23,41]. The amide I band is particularly important for evaluating protein secondary structure because it mainly corresponds to the C=O stretching of peptide bonds, and its position can indicate the dominant molecular conformation [23,41]. For the pure SF film, the amide I peak at 1621 cm^{-1} may be associated with a β-sheet conformation [23,41], while the amide II band, related to N–H bending and C–N stretching, and amide III band were observed at 1514 cm^{-1} and 1231 cm^{-1}, respectively.

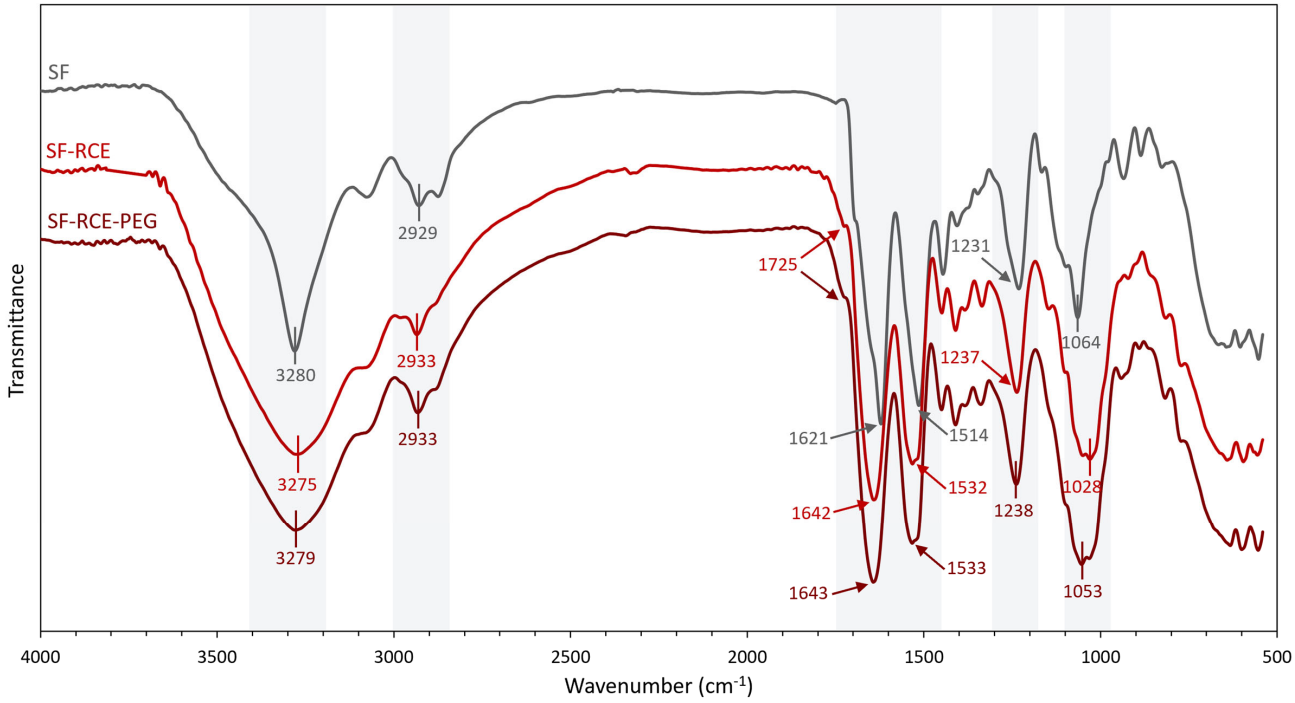


Figure 5. FTIR-ATR spectra of SF, SF-RCE, and SF-RCE-PEG films.

After incorporation of RCE and PEG 200, broader and more intense absorption in the 3200–3400 cm^{-1} region appeared, which can be attributed to contribution of hydroxyl-rich phenolic compounds from RCE and hydroxyl groups from PEG 200. Changes in the amide I region were also observed, suggesting contributions of C–O aromatic ring vibrations of phenolic compounds, and were manifested as a shift in the amide I band to higher wavenumbers (1642 cm^{-1} for SF-RCE and 1643 cm^{-1} for SF-RCE-PEG). These wavenumbers are typically associated with less ordered conformations (random coil and/or α-helix) [23,41]. Quantitative determination of the relative fractions of individual secondary structures would require deconvolution of the amide I band. Similar shifts of about 20 cm^{-1} and 10 cm^{-1} were also detected in the amide II and amide III regions, respectively. In the spectra of films containing RCE, regardless of the presence of PEG 200, two additional bands at 1028 cm^{-1} and 1725 cm^{-1} were observed and can be assigned to aromatic ring C-H deformation and C=O stretching vibration, respectively, as reported in previous studies on RCE-containing systems [53,55].

The FTIR-ATR results showed the persistence of the characteristic fibroin amide bands in all films confirming that fibroin backbone remained chemically intact. Moreover, the appearance of RCE-related bands certified successful incorporation of RCE into the SF matrix through mainly physical interactions, suggesting that the chemical functionality of the RCE and thus its pH responsiveness were not affected.

3.3.5. Colorimetric Response of Indicator Films to Volatile Ammonia

Volatile ammonia was used to simulate alkaline nitrogen compounds released during meat spoilage. The sensitivity and responsiveness of the colorimetric indicator films to ammonia vapor were evaluated by exposing the films to vapors generated from ammonia solution for 120 min in a closed environment. The film color changes were assessed by CIE Lab color analysis, including calculation of ΔE. The color transitions of the studied films are presented in Figure 6a. As shown in Figure 6a, the SF-RCE film gradually changed from magenta to darker purple shades and finally to a dark greenish tone after 120 min. In contrast, the SF-RCE-PEG film exhibited an earlier and more pronounced color change, reaching violet after 10 min and green after 60 min. The color shifts of the SF-RCE-PEG film were more consistent with those observed for RCE solutions (Figure 2a).

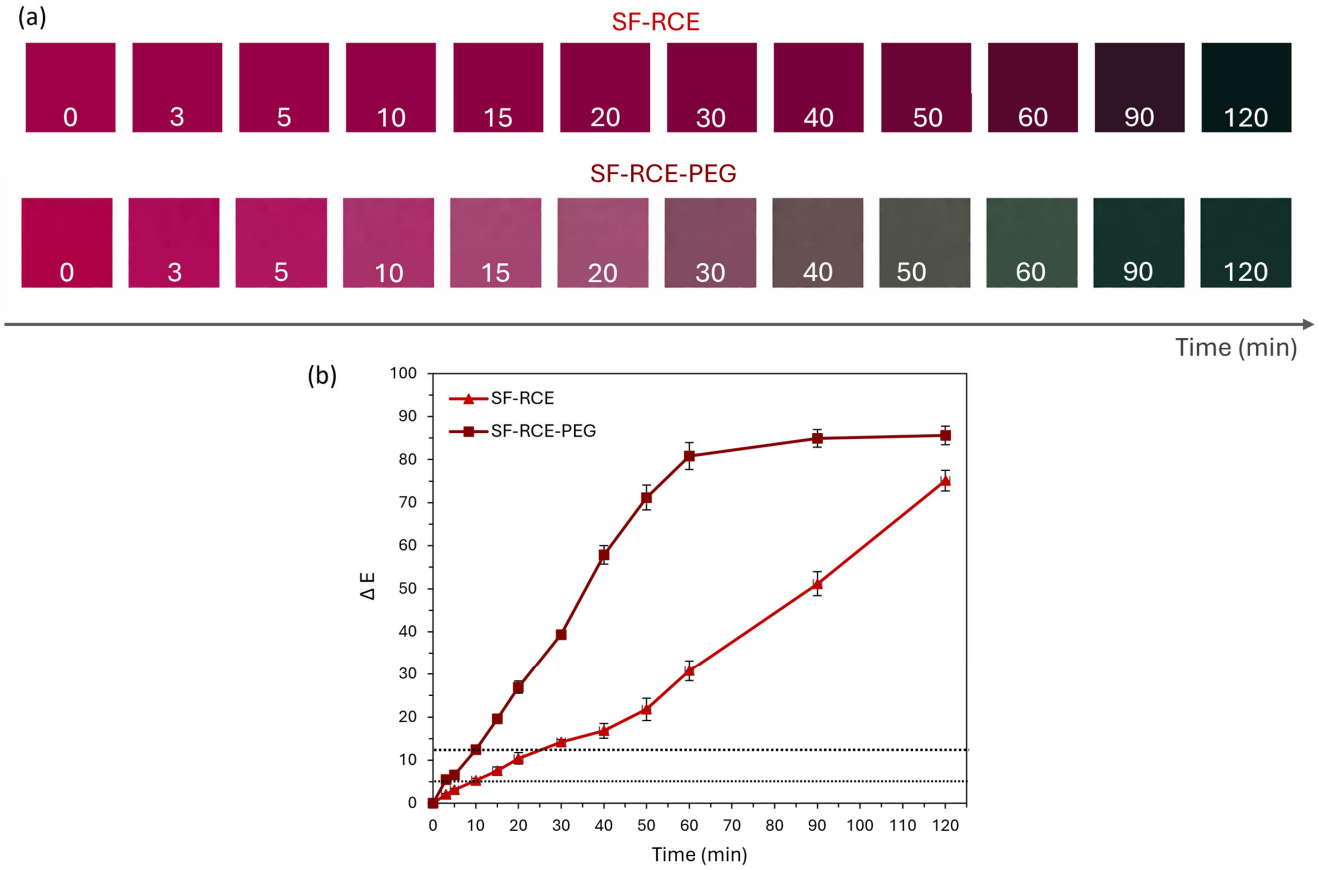


Figure 6. (**a**) Color response and (**b**) total color difference of SF-RCE and SF-RCE-PEG indicator films to ammonia vapor. Error bars represent the standard deviations ($n = 3$).

The described visual changes were confirmed by the ΔE values, which increased continuously for both samples during ammonia exposure, but with markedly different kinetics, as shown in Figure 6b. In general, ΔE values greater than 5 indicate a clearly perceptible color difference, whereas ΔE values greater than 12 correspond to a color from a different color space [3,9,55]. For the SF-RCE-PEG film, ΔE exceeded 5 within the first 3 min

and 12 after 10 min, then reached approximately 80 at 60 min and approached a plateau around 85 after 90–120 min of exposure time. In contrast, the SF-RCE film responded more slowly, reaching ΔE = 5 at 10 min and ΔE = 12 after 30 min; after 60 min, ΔE increased more steeply, reaching approximately 75 after 120 min of exposure to ammonia vapor.

The observed color changes may be attributed to ammonia hydrolysis and its conversion into $NH4^+$ and OH^-, with OH^- inducing structural transformations of anthocyanins and, consequently, changes in film color [8,54,56]. Also, the results suggest that PEG 200 enhanced the responsiveness of the SF-RCE-PEG film to ammonia vapors. This improvement may be related to PEG 200 plasticizing effect, which could increase polymer chain mobility and potentially facilitate ammonia diffusion and its interaction with the incorporated anthocyanins. However, further investigations are needed to confirm this proposed mechanism.

3.3.6. Colorimetric Response of Indicator Films During Chicken Meat Storage

The potential application of the indicator films for monitoring meat freshness was evaluated by exposing the films to the headspace of chicken breast for 96 h at room temperature. The color changes of the SF-RCE-PEG film are presented in Figure 7a,b. The film color noticeably changed each day, shifting from the initial magenta toward purple and becoming grayish-purple after 96 h. This transition is consistent with the behavior observed for RCE solutions and the SF-RCE-PEG film exposed to ammonia vapor (Figures 2a and 6a). As shown in Figure 7d, the ΔE values of the SF-RCE-PEG film increased progressively during chicken meat storage, following a similar trend to the NH_3-associated MIMS signal. At 24 h, ΔE reached approximately 20, which is well above the visual perceptibility limit [3,9,55], while the MIMS measurement indicated an increase in NH_3 concentration of approximately 900 ppm. With prolonged storage, both parameters, the ΔE of the SF-RCE-PEG film and NH_3 concentration, increased further. ΔE reached 58 at 96 h, while the increase in NH_3 concentration estimated from the MIMS measurement was approximately 20,000 ppm. The progressive color transition and the similar trends observed for ΔE and the NH_3-associated MIMS signal suggest that the SF-RCE-PEG film has potential as a visual indicator for monitoring changes in the headspace atmosphere during meat storage under improper storage conditions (i.e., temperatures exceeding recommended storage values). However, the MIMS measurements were performed on a single experimental sample; the obtained results should therefore be considered preliminary. In addition, water vapor may contribute to the MIMS signal at m/z 17, and a specific correction for this interference was not performed in the present study. Further measurements using independent samples are needed to confirm the observed trend and its relationship with the colorimetric response of the films. It should also be noted that NH_3 concentration alone does not provide a reliable measure of meat spoilage, which involves various microbiological and biochemical changes. Although the observed color changes demonstrate the response of the SF-RCE-PEG film to changes in the headspace atmosphere during meat storage, they cannot be directly correlated with the degree of meat spoilage. Further studies including total viable count (TVC) and TVB-N would be necessary to establish a reliable relationship between the colorimetric response and chicken meat freshness.

In contrast to the SF-RCE-PEG film, the SF-RCE film exhibited pronounced physical instability during the first 24 h of chicken meat storage. As shown in Figure 7c, the SF-RCE film largely retained its initial magenta color, while numerous bubble-like structures appeared on the film surface. After 24 h, the SF-RCE film disintegrated and partially solubilized. This behavior suggests that the non-plasticized SF-RCE film was unstable under high-moisture conditions generated by the meat and may have been affected by acidic metabolites also produced during meat spoilage [57]. This observation highlights the

importance of plasticizer addition for maintaining matrix stability and structural integrity during chicken meat storage monitoring.

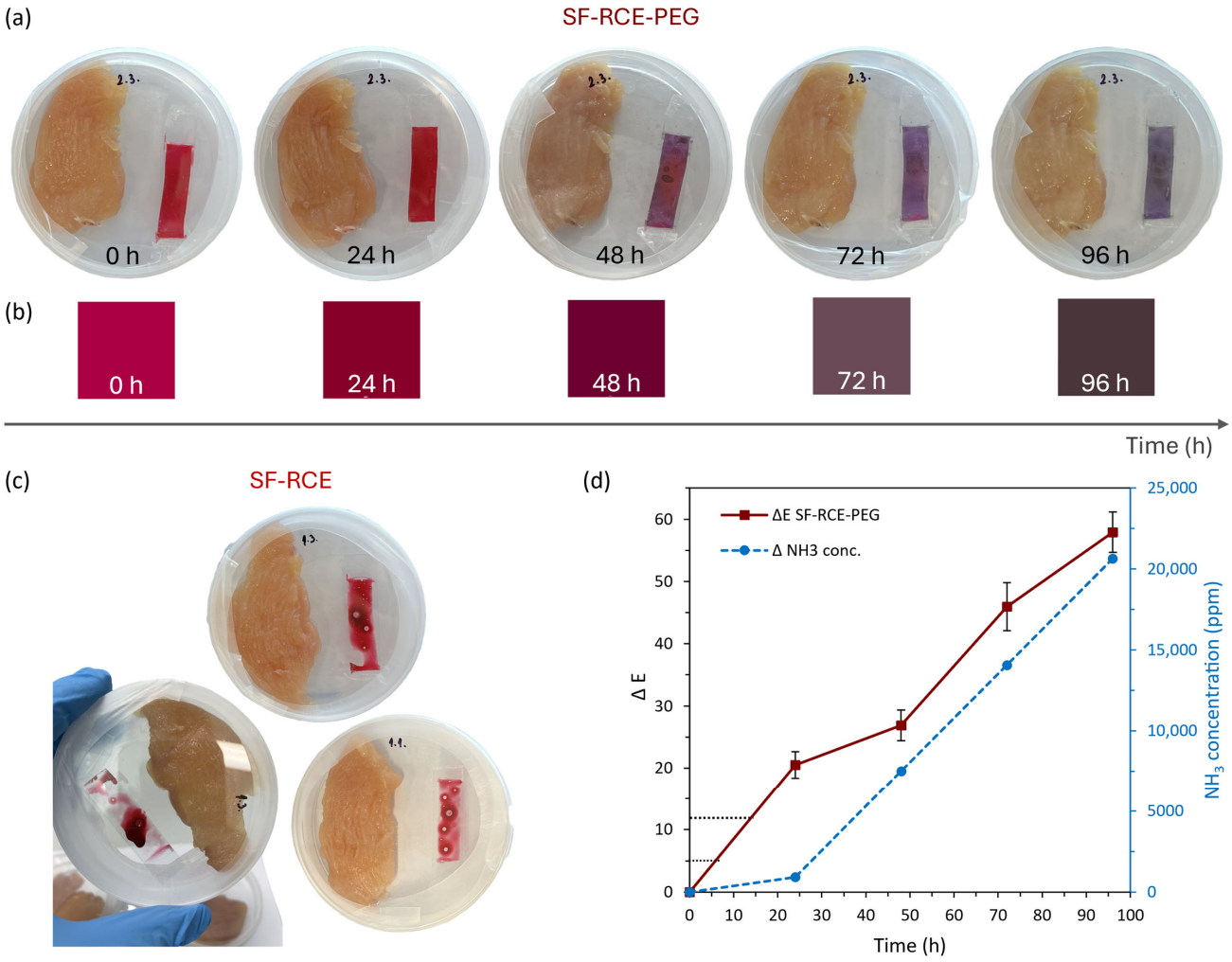


Figure 7. (**a**,**b**) Color change of SF-RCE-PEG indicator film, (**c**) behavior of SF-RCE indicator film, and (**d**) total color difference of SF-RCE-PEG indicator film and ammonia concentration change during chicken breast freshness monitoring.

4. Conclusions

In this study, water-based RCE, as an anthocyanin-rich component, was successfully incorporated into an SF matrix to fabricate pH-responsive indicator films. SEM analysis of the films showed that the incorporation of RCE increased structural heterogeneity compared with the neat SF film, whereas the additional incorporation of PEG 200 improved compatibility of the components and reduced localized stratification. TGA demonstrated that the neat SF film exhibited the highest thermal stability, while RCE incorporation led to a more complex degradation profile and promoted decomposition at lower temperatures. Nevertheless, all films showed thermal stability suitable for potential food packaging applications. FTIR-ATR spectroscopy confirmed the protein nature of the films and indicated that RCE was incorporated into the SF matrix predominantly through physical interaction, suggesting that the chemical properties of the RCE—and thus its pH sensitivity—were not affected. Exposure of the indicator films to ammonia vapor induced a clear, time-dependent color response, which was faster and more pronounced for the plasticized film (SF-RCE-PEG). During the chicken meat storage test, the SF-RCE-PEG film exhibited a visually evident color

change, with the color difference showing a similar increasing trend to the NH_3-associated MIMS signal. Overall, the SF-RCE-PEG film showed potential as a colorimetric indicator of changes in the headspace atmosphere associated with chicken meat storage under improper storage conditions (e.g., temperatures exceeding recommended conditions when the cold chain is interrupted). However, independent spoilage indicators, such as TVB-N, meat pH, and microbial counts, were not evaluated in the present study. Further studies including these parameters, as well as evaluating film stability and food-contact safety, are necessary to establish a reliable relationship between the colorimetric response and meat freshness and to validate the potential application of the films.

Author Contributions: Conceptualization, N.O. and J.K.; methodology, N.O., M.K., D.I. and V.F.; formal analysis, N.O., M.K., D.I. and V.F.; investigation, N.O., M.K. and D.I.; writing—original draft preparation, N.O.; writing—review and editing, N.O. and J.K.; visualization, N.O.; supervision, J.K. All authors have read and agreed to the published version of the manuscript.

Funding: This research was funded by the Ministry of Science, Technological Development and Innovation of the Republic of Serbia, grants number 451-03-33/2026-03/200358 and 451-03-34/2026-03/200134.

Data Availability Statement: The original contributions presented in this study are included in the article. Further inquiries can be directed to the corresponding author.

Conflicts of Interest: The authors declare no conflicts of interest.

References

1. Dudnyk, I.; Janeček, E.-R.; Vaucher-Joset, J.; Stellacci, F. Edible Sensors for Meat and Seafood Freshness. *Sens. Actuators B Chem.* **2018**, *259*, 1108–1112. [CrossRef]
2. Torres-Giner, S.; Figueroa-Lopez, K.J.; Melendez-Rodriguez, B.; Prieto, C.; Pardo-Figuerez, M.; Lagaron, J.M. Emerging Trends in Biopolymers for Food Packaging. In *Sustainable Food Packaging Technology*; Athanassiou, A., Ed.; Wiley-VCH: Weinheim, Germany, 2021; pp. 3–33, ISBN 9783527820061.
3. Zia, J.; Mancini, G.; Bustreo, M.; Zych, A.; Donno, R.; Athanassiou, A.; Fragoulli, D. Porous PH Natural Indicators for Acidic and Basic Vapor Sensing. *Chem. Eng. J.* **2021**, *403*, 126373. [CrossRef]
4. Zhai, X.; Xue, Y.; Sun, Y.; Ma, X.; Ban, W.; Marappan, G.; Tahir, H.E.; Huang, X.; Wu, K.; Chen, Z.; et al. Colorimetric Food Freshness Indicators for Intelligent Packaging:Progress, Shortcomings, and Promising Solutions. *Foods* **2025**, *14*, 2813. [CrossRef]
5. de Oliveira, T.V.; de Freitas, P.A.V.; Pola, C.C.; da Silva, J.O.R.; Diaz, L.D.A.; Ferreira, S.O.; Soares, N.d.F.F. Development and Optimization of Antimicrobial Active Films Produced with a Reinforced and Compatibilized Biodegradable Polymers. *Food Packag. Shelf Life* **2020**, *24*, 100459. [CrossRef]
6. Nastiti, P.W.; Bintoro, N. Classification of Freshness Levels and Prediction of Changes in Evolution of NH_3 and H_2S Gases from Chicken Meat during Storage at Room Temperature. *Agric. Eng.* **2022**, *11*, 90–98. [CrossRef]
7. Zhang, X.; Lu, S.; Chen, X. A Visual PH Sensing Film Using Natural Dyes from *Bauhinia blakeana* Dunn. *Sens. Actuators B. Chem.* **2014**, *198*, 268–273. [CrossRef]
8. Zhai, X.; Shi, J.; Zou, X.; Wang, S.; Jiang, C.; Zhang, J.; Huang, X.; Zhang, W.; Holmes, M. Novel Colorimetric Films Based on Starch/Polyvinyl Alcohol Incorporated with Roselle Anthocyanins for Fish Freshness Monitoring. *Food Hydrocoll.* **2017**, *69*, 308–317. [CrossRef]
9. Prietto, L.; Mirapalhete, T.C.; Pinto, V.Z.; Hoffmann, J.F.; Vanier, N.L.; Lim, L.T.; Guerra Dias, A.R.; da Rosa Zavareze, E. PH-Sensitive Films Containing Anthocyanins Extracted from Black Bean Seed Coat and Red Cabbage. *LWT-Food Sci. Technol.* **2017**, *80*, 492–500. [CrossRef]
10. Lee, J. Determination of Total Monomeric Anthocyanin Pigment Content of Fruit Juices, Beverages, Natural Colorants, and Wines by the PH Differential Method: Collaborative Study. *J. AOAC Int.* **2005**, *88*, 1269–1278. [CrossRef]
11. Giusti, M.M.; Wrolstad, R.E. Characterization and Measurement of Anthocyanins by UV-Visible Spectroscopy. In *Current Protocols in Food Analytical Chemistry*; John Wiley & Sons, Inc.: Hoboken, NJ, USA, 2001.
12. Teng, Z.; Jiang, X.; He, F.; Bai, W. Qualitative and Quantitative Methods to Evaluate Anthocyanins. *eFood* **2020**, *1*, 339–346. [CrossRef]
13. Ahmed, M.; Bose, I.; Nousheen; Roy, S. Development of Intelligent Indicators Based on Cellulose and *Prunus domestica* Extracted Anthocyanins for Monitoring the Freshness of Packaged Chicken. *Int. J. Biomater.* **2024**, *2024*, 7949258. [CrossRef]

14. Xu, Z.; Yu, X.; Liu, W.; Cheng, J.; Xiong, G. PH-Responsive Indicator Films Contained Composite Anthocyanins for Monitoring Meat Freshness. *Food Chem. X* **2025**, *27*, 102487. [CrossRef]
15. Xiong, G.; Zhou, X.; Zhang, C.; Xu, X. A Comprehensive Review of Intelligent Packaging Materials Based on Biopolymers: Role of Anthocyanins, Type and Properties of Materials, and Their Application in Monitoring Meat Freshness. *Int. J. Biol. Macromol.* **2024**, *282*, 137462. [CrossRef]
16. Chandrasekhar, J.; Madhusudhan, M.C.; Raghavarao, K.S.M.S. Extraction of Anthocyanins from Red Cabbage and Purification Using Adsorption. *Food Bioprod. Process.* **2012**, *90*, 615–623. [CrossRef]
17. Zhao, Z.; Li, Y.; Xie, M. Silk Fibroin-Based Nanoparticles for Drug Delivery. *Int. J. Mol. Sci.* **2015**, *16*, 4880–4903. [CrossRef]
18. Sashina, E.S.; Bochek, A.M.; Novoselov, N.P.; Kirichenko, D.A. Structure and Solubility of Natural Silk Fibroin. *Russ. J. Appl. Chem.* **2006**, *79*, 869–876. [CrossRef]
19. Patel, M.; Dubey, D.K.; Singh, S.P. Phenomenological Models of *Bombyx mori* Silk Fibroin and Their Mechanical Behavior Using Molecular Dynamics Simulations. *Mater. Sci. Eng. C* **2020**, *108*, 110414. [CrossRef]
20. Partlow, B.P.; Tabatabai, A.P.; Leisk, G.G.; Cebe, P.; Blair, D.L.; Kaplan, D.L. Silk Fibroin Degradation Related to Rheological and Mechanical Properties. *Macromol. Biosci.* **2016**, *16*, 666–675. [CrossRef]
21. Rockwood, D.N.; Preda, R.C.; Yücel, T.; Wang, X.; Lovett, M.L.; Kaplan, D.L. Materials Fabrication from *Bombyx mori* Silk Fibroin. *Nat. Protoc.* **2011**, *6*, 1612–1631. [CrossRef]
22. Bucciarelli, A.; Greco, G.; Corridori, I.; Pugno, N.M.; Motta, A. A Design of Experiment Rational Optimization of the Degumming Process and Its Impact on the Silk Fibroin Properties. *ACS Biomater. Sci. Eng.* **2021**, *7*, 1374–1393. [CrossRef]
23. Kundu, J.; Chung, Y.; Kim, Y.H.; Tae, G.; Kundu, S.C. Silk Fibroin Nanoparticles for Cellular Uptake and Control Release. *Int. J. Pharm.* **2010**, *388*, 242–250. [CrossRef]
24. Lammel, A.S.; Hu, X.; Park, S.; Kaplan, D.L.; Scheibel, T.R. Controlling Silk Fibroin Particle Features for Drug Delivery. *Biomaterials* **2010**, *31*, 4583–4591. [CrossRef]
25. Tao, H.; Brenckle, M.A.; Yang, M.; Zhang, J.; Liu, M.; Siebert, S.M.; Averitt, R.D.; Mannoor, M.S.; Mcalpine, M.C.; Rogers, J.A.; et al. Silk-Based Conformal, Adhesive, Edible Food Sensors. *Adv. Mater.* **2012**, *24*, 1067–1072. [CrossRef]
26. Marelli, B.; Brenckle, M.A.; Kaplan, D.L.; Omenetto, F.G. Silk Fibroin as Edible Coating for Perishable Food Preservation. *Sci. Rep.* **2016**, *6*, 25263. [CrossRef]
27. Ma, Z.; Jing, P. Stabilization of Black Rice Anthocyanins by Self-Assembled Silk Fibroin Nanofibrils: Morphology, Spectroscopy and Thermal Protection. *Int. J. Biol. Macromol.* **2020**, *146*, 1030–1039. [CrossRef]
28. Li, Y.; Yao, L.; Zhang, L.; Zhang, Y.; Zheng, T.; Liu, L.; Zhang, L. Enhanced Physicochemical Stabilities of Cyanidin-3-O-Glucoside via Combination with Silk Fibroin Peptide. *Food Chem.* **2021**, *355*, 129479. [CrossRef]
29. Giang, T.T.; Kim, C.; Duc, T.; Ha, P.T.M.; Thi, D.; Tram, N. Green-Engineered PEI/PVA-Functionalized Silk Fibroin Nanoparticles for Heat-Stable Delivery of *Clitoria ternatea* L. Anthocyanins: Formulation, Characterization, and Sustainability Assessment. *ACS Omega* **2025**, *10*, 38703–38718. [CrossRef]
30. Xia, L.; Li, L.; Xiao, Y.; Xiao, F.; Liu, L.; Chen, X.; Li, X.; Wang, H. Active Colorimetric Bilayer Polycaprolactone-Eucalyptus Oil@silk Fibroin-Bayberry Anthocyanins (PCL-EO@SF-BAs) Membrane with Directional Water Transport (DWT) for Food Packaging. *J. Colloid Interface Sci.* **2023**, *651*, 356–367. [CrossRef]
31. Matzeu, G.; Naveh, G.R.S.; Agarwal, S.; Roshko, J.A.; Ostrovsky-snider, N.A.; Napier, B.S.; Omenetto, F.G. Functionalized Mouth-Conformable Interfaces for PH Evaluation of the Oral Cavity. *Adv. Sci.* **2021**, *8*, 2003416. [CrossRef]
32. Liu, Y.; Zhan, K.; Chen, J.; Dong, Y.; Yan, T.; Zhang, X.; Pan, Z. Controlled Fabrication of PH-Visualised Silk Fibroin–Sericin Dual-Network Hydrogels for Urine Detection in Diapers. *Gels* **2025**, *11*, 671. [CrossRef]
33. Kruger, N.J. The Bradford Method for Protein Quantitation. In *The Protein Protocols Handbook. Springer Protocols Handbooks*; Walker, J.M., Ed.; Humana Press: Totowa, NJ, USA, 2009; pp. 17–24.
34. Kostić, M.; Omerović, N.; Ilić, D.; Brkić, B.; Filipović, V.; Terzić, M.; Bajac, J.; Bajac, B. Pectin-Based PH-Sensitive Films Incorporating Cold-Pressed Elderberry Juice for Chicken Freshness Monitoring. *J. Food Meas. Charact.* **2026**, *20*, 4558–4568. [CrossRef]
35. HunterLab Inc. CIE Standard Observers and Calculation of CIE X, Y, Z Color Values. Available online: https://support.hunterlab.com/knowledgebase/article/KA-05446 (accessed on 22 May 2026).
36. CIE. *CIE Standard Illuminant D65*; International Commission on Illumination (CIE): Vienna, Austria, 2022.
37. CIE. *Colour-Matching Functions of CIE 1931 Standard Colorimetric Observer*; International Commission on Illumination (CIE): Vienna, Austria, 2019.
38. van der Walt, S.; Schönberger, J.L.; Nunez-Iglesias, J.; Boulogne, F.; Warner, D.J.; Yager, N.; Gouillart, E.; Yu, T. The scikit-image contributors Scikit-Image: Image Processing in Python. *PeerJ* **2014**, *2*, e453. [CrossRef]
39. Jiang, H.; Zhang, W.; Cao, J.; Jiang, W. Effect of Purple Sugarcane Peel Extracts on Properties of Films Based on Lemon Peel Waste Pectin and the Application in the Visible Detection of Food Freshness. *Food Hydrocoll.* **2022**, *133*, 107982. [CrossRef]

40. Zhang, J.; Kaur, J.; Rajkhowa, R.; Li, J.L.; Liu, X.Y.; Wang, X.G. Mechanical Properties and Structure of Silkworm Cocoons: A Comparative Study of *Bombyx mori*, *Antheraea assamensis*, *Antheraea pernyi* and *Antheraea mylitta* Silkworm Cocoons. *Mater. Sci. Eng. C* **2013**, *33*, 3206–3213. [CrossRef]
41. Huang, Y.; Bailey, K.; Wang, S.; Feng, X. Silk Fibroin Films for Potential Applications in Controlled Release. *React. Funct. Polym.* **2017**, *116*, 57–68. [CrossRef]
42. Yaiphabi, S.; Kabita, S.; Jibankumar, S.; Shamjetshabam, S.; Chanu, B.; Meinam, L.; Kumar, M.; Mishra, T.R.; Sunil, S.; Laishram, S.; et al. Thermal Study of *Bombyx mori* Silk Fibroin Film Obtained through Degumming Process for Biomaterial Application. *J. Therm. Anal. Calorim.* **2025**, *151*, 9023–9034. [CrossRef]
43. Feng, Y.; Lin, J.; Niu, L.; Wang, Y.; Cheng, Z.; Sun, X.; Li, M. High Molecular Weight Silk Fibroin Prepared by Papain Degumming. *Polymers* **2020**, *12*, 2105. [CrossRef]
44. Freddi, G.; Tsukada, M.; Beretta, S. Structure and Physical Properties of Silk Fibroin/Polyacrylamide Blend Films. *J. Appl. Polym. Sci.* **1998**, *71*, 1563–1571. [CrossRef]
45. Qi, Y.; Wang, H.; Wei, K.; Yang, Y.; Zheng, R.; Kim, I.S.; Zhang, K.-Q. A Review of Structure Construction of Silk Fibroin Biomaterials from Single Structures to Multi-Level Structures. *Int. J. Mol. Sci.* **2017**, *18*, 237. [CrossRef]
46. Zhang, F.; Yang, R.; Zhang, P.; Qin, J.; Fan, Z.; Zuo, B. Water-Rinsed Nonmulberry Silk Film for Potential Tissue Engineering Applications. *ACS Omega* **2019**, *4*, 3114–3121. [CrossRef]
47. Jiang, X.; Jiang, T.; Gan, L.; Zhang, X.; Dai, H.; Zhang, X. The Plasticizing Mechanism and Effect of Calcium Chloride on Starch/Poly(Vinyl Alcohol) Films. *Carbohydr. Polym.* **2012**, *90*, 1677–1684. [CrossRef]
48. Zhao, M.; Nuerjiang, M.; Bai, X.; Feng, J.; Kong, B.; Sun, F.; Li, Y.; Xia, X. Monitoring Dynamic Changes in Chicken Freshness at 4◦C and 25◦C Using PH-Sensitive Intelligent Films Based on Sodium Alginate and Purple Sweet Potato Peel Extracts. *Int. J. Biol. Macromol.* **2022**, *216*, 361–373. [CrossRef]
49. Choubaki, S.; Baghaei, H.; Nafchi, A.M. Smart Indicator for Fish Freshness Monitoring: A Chitosan/Gelatin/Zinc Oxide Nanoparticle Composite Incorporating Pomegranate Flower Anthocyanin Extract Nanocapsules. *Food Sci. Nutr.* **2025**, *13*, e70944. [CrossRef]
50. Li, M.; Tian, W.; Zhang, Y.; Song, H.; Yu, Y.; Chen, X.; Yong, N.; Li, X.; Yin, Y.; Fan, Q.; et al. Enhanced Silk Fibroin/Sericin Composite Film: Preparation, Mechanical Properties and Mineralization Activity. *Polymers* **2022**, *14*, 2466. [CrossRef]
51. Gutierrez-Contreras, R.; Fernandez-gutierrez, M.; Olalla-perez, P.; La Hoz, A.D.; Marcos, S. Comparative Analysis of Silk Fibroin Membranes across Cross-Linking Methods: Processing and Characterization. *ACS Omega* **2024**, *9*, 38452–38461. [CrossRef]
52. Zhao, M.; Qi, Z.; Tao, X.; Newkirk, C.; Hu, X.; Lu, S. Chemical, Thermal, Time, and Enzymatic Stability of Silk Materials with Silk I Structure. *Int. J. Mol. Sci.* **2021**, *22*, 4136. [CrossRef]
53. Silva-Pereira, M.C.; Teixeira, J.A.; Pereira-Júnior, V.A.; Stefani, R. Chitosan/Corn Starch Blend Films with Extract from *Brassica oleraceae* (Red Cabbage) as a Visual Indicator of Fish Deterioration. *LWT-Food Sci. Technol.* **2015**, *61*, 258–262. [CrossRef]
54. Freitas, P.A.V.; Silva, R.R.A.; De Oliveira, T.V.; Soares, R.R.A.; Junior, N.S.; Moraes, A.R.F.; Clarissa, A.; Pires, S.; Soares, N.F.F. Development and Characterization of Intelligent Cellulose Acetate-Based Films Using Red Cabbage Extract for Visual Detection of Volatile Bases. *LWT* **2020**, *132*, 109780. [CrossRef]
55. Devarayan, K.; Kim, B.-S. Reversible and Universal PH Sensing Cellulose Nanofibers for Health Monitor. *Sens. Actuators B Chem.* **2015**, *209*, 281–286. [CrossRef]
56. Jiang, G.; Hou, X.; Zeng, X.; Zhang, C.; Wu, H.; Shen, G.; Li, S. Preparation and Characterization of Indicator Films from Carboxymethyl-Cellulose/Starch and Purple Sweet Potato (*Ipomoea batatas* (L.) Lam) Anthocyanins for Monitoring Fish Freshness. *Int. J. Biol. Macromol.* **2020**, *143*, 359–372. [CrossRef]
57. Franke, C.; Beauchamp, J. Real-Time Detection of Volatiles Released During Meat Spoilage: A Case Study of Modified Atmosphere-Packaged Chicken Breast Fillets Inoculated with *Br. thermosphacta*. *Food Anal. Methods* **2017**, *10*, 310–319. [CrossRef]

Disclaimer/Publisher's Note: The statements, opinions and data contained in all publications are solely those of the individual author(s) and contributor(s) and not of MDPI and/or the editor(s). MDPI and/or the editor(s) disclaim responsibility for any injury to people or property resulting from any ideas, methods, instructions or products referred to in the content.